Discovery of Drug-like Ligands for the Mac1 Domain of SARS-CoV-2 Nsp3

Rajdeep S. Virdi, Robert V. Bavisotto, Nicholas C. Hopper & David N. Frick*

Department of Chemistry & Biochemistry

The University of Wisconsin- Milwaukee, Milwaukee, WI 53217

KEYWORDS: COVID-19, Antiviral Drug target, Severe Acute Respiratory Syndrome, Coronavirus.

Corresponding Author: David N. Frick, Department of Chemistry & Biochemistry, University of Wisconsin- Milwaukee, 3210 N Cramer St., Milwaukee, WI, USA, 53211.

frickd@uwm.edu.

ABSTRACT

The Mac1 domain of the multifunctional SARS-CoV-2 non-structural protein 3 (nsp3) is a potential COVID-19 drug target because it is suspected to enhance the ability of the virus to evade the human immune system. The SARS-CoV-2 Mac1 domain binds ADP-ribose and proteins harboring this important post-translational modification. Small molecules that bind the Mac1 domain in place of ADP-ribose might therefore be useful as molecular probes or scaffolds for antiviral drug discovery. Two high throughput screens were used here to identify such ligands in small libraries of drugs and drug-like compounds. The first screen used differential scanning fluorimetry (DSF, aka the thermal shift or ThermoFluor assay) to examine the melting temperature of SARS-CoV-2 Mac1 domain in the presence of various compounds. In the second screen, various high-resolution SARS-CoV-2 Mac1 structures were used with Autodock VINA to identify potential ligands. Numerous hit compounds were either steroids (estradiol valerate & flunisolide), beta-lactams (cefaclor & cefatrizine), or benzimidazoles (telmisartan, rabeprazole, omeprazole, & esomeprazole). Isothermal titration calorimetry was used to confirm that rabeprazole, omeprazole, and compounds in other chemical classes, such as irinotecan, nifedipine, trifluoperazine, bind SARS-CoV-2 Mac1 with an affinity similar to ADP-ribose.

Introduction.

Direct acting antivirals (DAAs) are desperately needed to treat COVID-19 patients and stem the devastation caused by the current Severe Acute Respiratory Syndrome Coronavirus 2 (SARS-CoV-2) pandemic. DAAs are typically developed from potent inhibitors of viral enzymes or high-affinity ligands of viral proteins. For example, the first FDA-approved DAA against SARS-CoV-2, remdesivir,[1] is a phosphoramidate prodrug that is converted to a nucleoside triphosphate non-obligate chain terminator that inhibits the SARS-CoV-2 RNA dependent RNA polymerase, halting SARS-CoV-2 replication.[2] Based on past experiences with other viruses, any effective DAA therapy will likely involve a cocktail of more than one antiviral agent because drug resistance evolves rapidly.[3–5] It is therefore essential that methods are developed to rapidly identify small-molecule drug-like ligands for as many SARS-CoV-2 proteins as possible. Even if such ligands are not developed into drugs, they will be useful as molecular probes to study the biological role of SARS-CoV-2 proteins. Such chemical genetics studies have, in the past, elucidated key cellular pathways, like those involved in regulating innate immunity.[6]

The ~29,900 nucleotide long positive-sense RNA SARS-CoV-2 genome, like that of other coronaviruses, encodes more structural and non-structural proteins than most RNA viruses. [7] These potential DAA targets include 16 nonstructural proteins (nsps), four structural proteins, six accessory proteins, and possibly other yet-to-be identified products produced from the 29 putative SARS-CoV-2 open reading frames.[8] Many targets are unique to coronaviruses, such as the 3'-5' exonuclease that proofreads RNA synthesis.[9] Most of the nsps are products of the rep1b open-reading frame that encode a short (*aka* ORF1a) and long (*aka* ORF1b) polyprotein due to that fact that an internal RNA hairpin occasionally causes translational frameshifting.

Several coronavirus proteases cleave the ORF1a polyprotein into nsp1 to nsp10, and the ORF1b polyprotein into nsp1 through nsp16. The subject of this study is the multifunctional 945 amino-acid-long nsp3 protein that cleaves the three junctures separating nsp1, nsp2 and nsp3.[10]

If SARS-CoV-2 nsp3 behaves in the same way in the cell as its homologs from other coronaviruses, it is most likely tethered to the ER lumen by two transmembrane helices with most of the protein in the cytoplasm. On the N-terminal side of the transmembrane domains (TMs) reside two ubiquitin-like domains (Ubl1 and Ubl2), two papain-like protease domains ($PLP1^{pro}$ and $PLP2^{pro}$), three macrodomains (Mac1, Mac2, and Mac3), a nucleic-acid-binding domain (NAB), and a hypervariable region (HVR), assembled in the order: Ubl1-HVR-$PLP1^{pro}$-Mac1-Mac2-Mac3-DPUP- $PLP2^{pro}$-NAB-G2M-TM, where DPUP is a "Domain Preceding Ubl2 and $PL2^{pro}$" and G2M is a "group 2- specific marker." Two domains, Y1 and CoV-Y, of unknown function reside on the C-terminal side of the nsp3 TMs.

In a previous study, Frick *et al.*[11] characterized the SARS-CoV-2 Mac1 domain (aka the "X" domain), primarily because it is the most different nsp3 domain from its nearest relative, SARS-CoV.[12] This domain binds ADP-ribose and has a weak hydrolytic activity[13] that removes ADP-ribose that is covalently attached to proteins.[14] Claverie recently proposed that this activity might be linked to the Cytokine Storm Syndrome commonly found in Covid-19 patients.[15] Here, we report the results of a screening campaign designed to find drug-like Mac1 domain ligands, which might facilitate DDA design or which could be useful molecular probes. Two high-throughput screens were designed to identify such ligands. Both were used to screen libraries of drugs and drug-like compounds including the National Institutes of Health (NIH) clinical

collection (726 compounds) and the National Cancer Institute (NCI) mechanistic set (540 compounds). The first assay used differential scanning fluorimetry (DSF, aka the thermal shift, or ThermoFluor assay)[16–18] methods to examine the melting temperature (T_m) of SPYRO Orange-saturated SARS-CoV-2 Mac1 in the presence of each compound in an assay that can be performed in standard quantitative PCR thermocyclers. In an orthogonal screen, various high-resolution Mac1 domain structures were used with AutoDock VINA[19] to identify compounds binding with highest affinity to all structures. Using ADP-ribose, which raised the melting temperature of SARs-CoV-2 Mac1, as a positive control, the DSF assay was optimized for HTS to yield Z'-Factors between 0.5 and 0.75. In the screen of the NCI and NIH collections, about 1% and 5% of compounds tested influenced apparent melting temperature, respectively. However, the majority did so by altering SPYRO Orange fluorescence. After identifying and excluding such interfering compounds, hits were tested at 0.5 mM in triplicate, and in concentration response assays. Interestingly, several confirmed DSF assay hits also had some of the best docking scores, and molecular models predict that the most promising candidates bind in the ADP-binding cleft of the Mac1.

Materials and Methods

Purified SARS-CoV-2 Mac1 protein was prepared as described previously.[11]

Differential Scanning Fluorimetry (DSF) – Assays were performed in 96-well PCR plates using an Eppendorf Mastercycler ep Realplex Quantitative Realtime PCR System with each well containing 19 µl of Master-mix and 1 µl of compound stock at 10 mM. The master-mix was prepared by adding 20 µl of 500 µM Mac1, 2.5 µl 5000x SPYRO Orange protein gel stain (Sigma-

Aldrich catalog #S5692) and 1977.5 µl of buffer (20 mM MOPS, 25 mM NaCl, pH 7) with a final volume of 2 ml. The 96-well PCR plate was then sealed with clear adhesive film and centrifuged at 1,100 RPM for 5 mins. In the thermocycler, the temperature was raised from 20 °C to 95 °C at a rate of 2 °C per min while measuring fluorescence in the "TAMRA" channel. Each plate included both negative (DMSO) and positive (ADP-ribose) controls. T_m's were calculated either by finding the peaks in plots of *d*F/*d*T vs T, or by fitting the data to equation 1 using either GraphPad Prism or TSA-craft (https://sourceforge.net/projects/tsa-craft/).[20]

$$F_{obs} = F_{min} \frac{F_{max} - F_{min}}{1 + e^{\left(\frac{T_m - T}{a}\right)}} \qquad \text{(Equation 1)}$$

In Eq. 1, F_{obs} is the observed fluorescence at each temperature (T), F_{min} is the minimum observed fluorescence, F_{max} is maximum observed fluorescence, and a is a *Hill* slope.

Compound EC_{50} value were determined in a similar way as for the initial screening but by varying the concentration of each compound. Concentration-response assays were also performed in 96-well PCR plates with 19 µl of Mastermix with 1 µl of the highest concentration of the compound in the first row and lowest concentration in last row. Observed T_m values ($T_{m\ obs}$) at each compound concentration (L) were fit to equation 2.

$$T_{m\,obs} = \frac{\Delta T_{m\,max} * [L]}{EC_{50} + [L]} + T_m \qquad \text{(Equation 2)}$$

In equation, $\Delta T_{m\ max}$ is the maximum change in T_m, where T_m is the melting temperature of the protein in the absence of compounds, and EC_{50} is the ligand concentration causing a change in T_m that is half of $\Delta T_{m\ max}$.

Molecular Modeling & Virtual Screening— Computational ligand screening was performed on various forms of the Mac1 protein, including both the unliganded (6WEY and

6VXS) and ADP-ribose-bound forms (6W02), using the program AutoDock VINA.[19] These protein structures were computationally screened with NCI mechanistic set (library 1) and the NIH clinical collection NCI (library 2). The protein files were downloaded directly from the protein data bank and processed as follows before submitting for screening. All solvent molecules (HETATM) were removed from the files. Polar hydrogen atoms were added and Kollman charges were included in the protein files. The converted protein and ligand file libraries (both pdbqt files) were uploaded to a parallel computing cluster and run with the following parameters: Energy difference = 4; Number of recorded modes = 20; Exhaustiveness was set to 12. Docking box location was configured prior to using AutoDock tools. After the docking calculation was complete, the locations, orientations, and binding affinities of the top candidates were examined by the aid of UCSF Chimera and tabulated for comparison.

Isothermal Titration Calorimetry (ITC)— Binding of selected hit compounds to SARS-CoV-2 Mac1 was measured using a Nano ITC (TA Instruments). Before starting the measurement, samples of both ligand and protein were diluted in 10 mM MOPS, 10 mM NaCl at pH 7 and were degassed at 400 mmHg for 30 minutes. Measurements were taken at 20 °C by injecting 2.0 µl aliquots of 1 mM of the compound to 50 µM protein (175 µl initial volume) with 200 rpm stirring rate. Using NanoAnalyze Software (v. 3.11.0), data were fitted by non-linear regression to an independent binding model. Briefly, after baseline correction, background heats from ligand-to-buffer titrations were subtracted, used to find best fit parameters for the stoichiometry of the binding (n), free energy of binding (ΔG), apparent enthalpy of binding (ΔH), and entropy change (ΔS). Dissociation constants (K_d) were calculated from the ΔG.

Results

DSF has been used before to study ligand binding to viral macrodomain proteins, including the homologous Mac1 domains encoded by MERS,[21] chikungunya, and Venezuelan equine encephalitis viruses.[22] DSF was also used to identify ligands for the fragment-based design of potent inhibitors of ADP-ribosylation enzymes called tankyrases.[23] In DSF experiments using SARS-CoV-2 Mac1, the presence of ADP-ribose raised the Mac1 melting temperature from 52 °C to almost 60 °C in a concentration-dependent manner (Fig. 1A). Melting curves in thermal-shift assays can be analyzed either by directly fitting the data using non-linear regression (Eq. 1A, Fig. 1A) or by finding the peaks on plots of the first derivative of the melting curve (Fig. 1B). Both methods yield similar T_m values in the presence and absence of ADP-ribose (Fig. 1C). When the resulting T_m values are fit to a binding equation (Eq. 2, methods), best-fit concentrations causing 50% response (EC_{50}) are similar to, but consistently higher than, the dissociation constants calculated from direct binding experiments performed in similar buffers using isothermal titration calorimetry (ITC). The K_d values found in ITC experiments for ADP-ribose binding by Mac1 are typically 5-10 times lower than the corresponding EC_{50} values, most likely because DSF does not directly measure binding, but rather the ability of a ligand to alter the interaction of a fluorescent reporter dye with the protein of interest.

After confirming that ADP-ribose is an acceptable positive control for a Mac1 high-throughput screen (HTS) utilizing DSF as a readout, assay conditions were varied to optimize the assay. First, the effect of dimethyl sulfoxide (DMSO) was examined. DMSO did not change the melting curve even at concentrations as high as 10% (v/v) (data not shown). Next, titrations with ADP-ribose were repeated in various buffers, with pH ranging from 6.5 to 8.0. Similar

results were obtained in all buffers with no significant differences noted, either in maximal ΔT_m, or apparent affinity for ADP-ribose (Fig. 1D). Likewise, divalent cations did not influence either EC_{50} values for ADP-ribose or maximal ΔT_m values (Fig. 1E), which was a somewhat surprising result for a nucleotide-binding protein, and putative hydrolase. In contrast, the ionic strengths of the assay buffers influenced the results, with the largest ΔT_m values and lowest EC_{50} values being obtained at the lowest ionic strengths (Fig. 1F). Based on these results, DSF assays were subsequently performed in 20 mM MOPS pH 7 buffer containing 25 mM NaCl. Some salt was included to reduce possible non-specific interactions with ligands.

The purified SARS-CoV-2 Mac1 protein was then titrated with various nucleotides similar to ADP-ribose to determine if the DSF assay recapitulates the structure-activity relationships observed in prior ITC studies (Table I).[11] All nucleotides tested were previously shown to bind Mac1, except AMP. The main differences observed with ITC reflected the fact that binding of only ADP-ribose was enthalpy driven, while the other nucleotides were bound by Mac1 with smaller decreases in enthalpy, but with counterbalancing decreases in binding entropy so that the free energy changes (and K_d) were similar to ADP ribose. [11] Most nucleotides caused T_m to change, with the notable exception of ADP-glucose, which did not. Unlike K_d values measured in ITC experiments, the EC_{50} values for each nucleotide were different, with ADP-ribose having a notably lower EC_{50} value than all other nucleotides (Table I).

The first pilot screen was performed using compounds from the National Cancer Institute Mechanistic Diversity Library (NCI, https://dtp.cancer.gov/repositories/)(Fig. 2A)[24] and the second with the NIH clinical collection (https://commonfund.nih.gov/molecularlibraries/tools) (Fig. 2B).[25] Each compound was tested

at 0.5 mM such that the final DMSO concentration in each assay was 5% (Fig. 2A). Each 96-well plate contained 80 wells of test compounds, eight negative control (5% DMSO only) and eight positive controls with 0.5 mM ADP-ribose. Although differences between positive and negative controls were relatively small, Z' factors[26] were always above 0.5 for each plate and typically above 0.7 (0.72 for the data in Fig. 2C). Plate-to-plate variability was negligible (Fig. 2C).

Melting curves obtained from each DSF assay were analyzed to calculate the T_m values in two ways. In the first, the peak of a plot of the first derivative vs. temperature was found using standard software (Microsoft Excel and/or GraphPad Prism). In the second, the data were fit to Eq. 1 (methods) using GraphPad Prism or specialized program TSA-CRAFT.[20] For the NIH clinical library, the two method yielded similar T_m values for 99% (534/540) of the compounds tested (Fig. 2D), while the results were more variable for the NIH library, where curves for 46 of the 726 compounds tested (6%) gave different T_m values using by the two techniques (Fig. 2E). Most of the differences occurred because the tested compounds produced unusual melting curves, with multiple peaks and valleys. The TSA-CRAFT software package incorporates an algorithm that identifies such abnormal curves, and when they were eliminated, only nine compounds had notably different T_m values when the data were analyzed using both the direct-fit and first-derivative methods (Fig. 2E). These abnormal melting curves correlated with compounds that interfere with assay fluorescence, either because they fluoresce themselves, or enhance fluorescence of the SPYRO Orange reporter dye. As shown in Fig. 2F, such interfering compounds can also be identified by plotting T_m's versus the initial fluorescence seen in the melting curve.

Only one compound in the NCI set raised the T_m value of SARS-CoV-2 Mac1 protein; NSC 635448, which is a copper bromide complex (Copper, bromo[2-[1-(2-pyridinyl)ethylidene][N,N-dimethyl-hydrazinecarbothioamidato-N,N,S]-Hydrazinecarbothioamide), and was not pursued further. In contrast, 12 compounds in the NIH collection significantly increased the melting temperature of Mac1. Two noteworthy hits relevant to current COVID-19 research were the ACE inhibitor telmisartan[27] and two steroids, estradiol valerate and the anti-inflammatory corticosteroid flunisolide (Fig. 3).[28, 29]

In the orthogonal "virtual" screen, the recently deposited SARS-CoV-2 Mac1 crystal structures (PDB files 6WEY, 6W02, and 6VXS) were use as targets in the program AutoDock Vina (Fig. 4). The PDB file 6W02 is a co-structure with ADP-ribose, but the other two were done in the absence of ADP-ribose. Each was searched free from ligands. All compounds in the NCI and NIH libraries were screened with each protein structure. For files 6W02 and 6VXS, each ligand was docked with two chains in the asymmetric unit (*i.e.* BioAssembly (A and B)), separately treating the protein as a monomer. Similar minimal binding energies were obtained with each structure (Fig. 4A). The structure used in the screens did not greatly influence the hits returned. This is not surprising, since the protein does not drastically alter its conformation upon binding ADP-ribose. Interestingly, telmisartan was again identified as a possible SARS-CoV-2 Mac1 ligand (Fig. 4A). The only compounds with larger binding energies were the topoisomerase inhibitor irinotecan (Fig. 3D),[30] and the RNA synthesis inhibitor dactinomycin (actinomycin D), another drug recently proposed act as a COVID-19 treatment.[31] Irinotecan did not significantly alter the T_m value of SARS-CoV-2 Mac1, and dactinomycin produced abnormal melting curves (Fig. 4B).

Plots of binding energies *vs*. T_m (Fig. 4B) helped to identify compounds for follow-up assays. First, several compounds were selected for cherry-pick and concentration response assays (red, green circles, Fig. 4B). Although many of the compounds that yielded high T_m values reproduced the them upon cherry-picking, their concentration-response curves often looked unusual. For example, addition of estradiol valerate led to flattened regions with sharp peaks, suggesting that TSA-CRAFT might not successfully flag all abnormal melting curves (Fig. 4C). In the NIH collection, 27 compounds were identified that yielded consistently lower than typical melting temperatures. Although ligands that reduce a protein's T_m are often assumed to bind and stabilize unfolded structures,[32] we nevertheless examined some of these hits in more detail. Interestingly, many hits that lowered T_m values were members of similar chemical classes. For example, two were lactam antibiotics (Fig. 3B), and a several others were benzimidazoles chemically resembling telmisartan (Fig. 3C). Many reproduced well upon cherry-picking (Fig. 4B) and depressed the T_m values when interacting with SARS-CoV2 Mac1 in a concentration-dependent manner (Fig. 4D, 4E).

Binding sites were not restricted in each virtual screening search (Fig. 5) but, for most compounds, minimal binding energy (best fit) values were obtained for structures in which the compound docked near the ADP-ribose binding site. Close examination of molecular models generated by AutoDock Vina reveal that the steroids (Fig. 5A), β-lactams (Fig. 5B) and benzimidazoles (Fig. 5C) can each occupy the ADP-ribose-binding cleft on SARS-CoV-2 Mac1. The larger compounds in each class make more contacts with amino acids in the cleft, explaining their higher binding energies. If these compounds are confirmed as effective ligands, their structures might be useful to guide the rational design of higher-affinity derivatives.

After confirming the results with fresh compounds, ITC was used as a second orthogonal assay to examine protein-ligand binding. Unfortunately, conditions could not be found to produce isotherms for either the steroids or the lactams, so none of those compounds could be confirmed as ligands with ITC. In contrast, some of the benzimidazoles were found to bind in ITC experiments with dissociation constants similar to their EC_{50} values from DSF (Table II, Fig. 6A). Irinotecan was also confirmed to bind to SARS-CoV-2 using ITC (Fig. 6B), as well as two other drugs that depressed T_m; the antipsychotic trifluoperazine (Fig. 6C), and the calcium channel blocker nifedipine (Fig. 6D).

Discussion

The idea that SARS-CoV Mac1 might function as an enzyme in the cell to remove ADP-ribose from antiviral proteins is intriguing, and if verified, would identify an important new drug target for COVID-19.[15] The goal of this project was to facilitate those efforts by developing a high-throughput assay to identify compounds that bind SARS-CoV-2 Mac1 in place of ADP-ribose. Such compounds could be used as molecular probes or scaffolds for antiviral drug development. A thermal shift binding assay was use here because it is inexpensive and direct. DSF's main disadvantage is that it requires relatively large amounts of protein. This a minor concern because of the ease with which Mac1 can be produced from *E. coli*,[11] but it limits the ability of the DSF assay to differentiate high-affinity from low-affinity ligands. The lowest EC_{50} value the DSF assay can measure is 3 µM because 6 µM protein is needed in the assay. The data presented here clearly show how the assay can be used to identify ligands for SARS-CoV-2 Mac1, and that several FDA approved drugs interact with the protein with affinities comparable to ADP-ribose.

The most attractive alternative to a DSF binding assay would be an enzyme assay that monitors the ability of Mac1 to hydrolyze ADP-ribose-based substrates.[33] Enzyme assays with SARS-CoV-2 Mac1 are more difficult to perform because the suspected biological substrates for coronavirus Mac1 proteins need to be synthesized first using ADP-ribosyl transferase enzymes. The enzymes suspected to produce such Mac1 substrates are in the poly(ADP-ribose) polymerase (PARP) class, and they use nicotinamide adenine dinucleotide (NAD) as the source of ADP-ribose. PARPs catalyze that transfer of ADP-ribose from NAD to amino acid side chains and the 3'OH of adenylate,[34] but some PARPs do not always technically act as polymerases. Instead they only transfer a single ADP-ribose to an amino acid. Curiously, only these "mono" ADP-ribosylated peptides typically are substrates for viral macro domains.[14] The advantage of an enzyme-based assay would be its ability to detect more potent inhibitors if it could be performed using low protein concentrations. There is some evidence that such an assay could be designed for SARS-CoV-2 Mac1 because a recent pre-print reports SARS-CoV-2 Mac1 can remove a single ADP-ribose from a protein.[37] Other macro domains remove ADP-ribose from proteins,[34, 35] and early studies, steady state kinetics were used to demonstrate catalytic activity for SARS-CoV Mac1 in assays monitoring the removal a 1''-phosphate from ADP-ribose with a K_m of 58 µM and a very slow k_{cat} of 5 min^{-1}.[13] However, notably faster rates have not yet been reported for peptide substrates.[35,36,37] These feeble activities stand in stark contrast to those of other cellular enzymes that degrade ADP ribose, such as the Nudix enzymes,[38] which degrade ADP-ribose with turnover rates and catalytic efficiencies several orders-of-magnitude higher than those observed with macrodomains.[39] Other nsp3 domains might accelerate a Mac1 enzymatic activity, as was demonstrated with the HEV nsp3 helicase and macrodomain.[35]

However, a completely different idea would be that ligand binding to Mac1 instead guides the nsp3 protease to cellular proteins to degrade, deubiquitinate, or catalyze the removal of Interferon-stimulated gene 15 proteins. High-affinity drug-like ligands might help test these ideas, and it might also be worthwhile to test if compounds reported here act synergistically with recently reported papain-like protease inhibitors targeting SARS-CoV-2 nsp3.[10]

The most interesting hits in these screens were the steroids and telmisartan (Fig. 3). There seems to be a clear sex difference in COVID-19 disease severity, and an interaction between a sex hormone and a SARS-CoV-2 protein might help explain this difference.[28, 29] Similarly intriguing is the possibility that the ACE inhibitor telmisartan, which shares the receptor needed for SARS-CoV-2 to infect cells, might be an antiviral.[27] Unfortunately, the poor aqueous solubility of the steroids and telmisartan confounded the ability to examine their interaction with SARS-CoV-2 Mac1. However, other benzimidazoles were also hits (Fig. 3C), and they could be verified as ligands using ITC (Fig. 6). Rabeprazole, omeprazole, and esomeprazole all elicit their antacid effects by targeting proton pumps, but there is no evidence that proton pump inhibitors affect the severity of COVID-19.[40] Similarly, no peer-review studies have been published reporting antiviral effects for the other three hits confirmed using ITC: nifedipine, trifluoperazine, and irinotecan. Caution should also be exercised because each verified compound lowered the apparent T_m of SARS-CoV-2 Mac1, indicating that they might bind the protein's unfolded state. It's worth noting, however, that similar destabilizing compounds were found to inhibit macrodomains in other assays not based on thermal shifts,[33] suggesting that the destabilizing compounds might bind a folded protein that assumes a different conformation. X-ray crystallography is presently being used to examine that possibility.

The next step in this project will be to examine the effect of hit compounds on cells harboring SAR-CoV-2 or surrogate reporter viruses. Some of the compounds above might inhibit SARS-CoV-2 replication based on the fact that Shimizu *et al.* showed that small molecules, found in virtual screens targeting the homologous nsp3 macrodomain from Chikungunya virus, inhibit replication of Chikungunya replicons.[41] However, further optimization would most likely be necessary for these probes to be useful in cellular studies. Fortunately, all hits reported here are FDA approved drugs with hundreds of analogs available to facilitate such work. Alternatively, this optimized DSF assay could be used to screen larger more diverse libraries for more attractive probe candidates.

Acknowledgements

The authors are grateful to Wilfred Tysoe and Nicholas Silvaggi, for helpful discussions and encouragement, and Daad Saffarini for allowing this work to proceed during the COVID-19 pandemic lockdown. This work was supported by University Wisconsin-Milwaukee's generous F&A cost return policy (National Institutes of Health Grant R01 AI088001) and is based upon work supported by the National Science Foundation under Grant Number CHE-1855199.

References

(1) Agostini, M. L.; Andres, E. L.; Sims, A. C.; Graham, R. L.; Sheahan, T. P.; Lu, X.; Smith, E. C.; Case, J. B.; Feng, J. Y.; Jordan, R.; Ray, A. S.; Cihlar, T.; Siegel, D.; Mackman, R. L.; Clarke, M. O.; Baric, R. S.; Denison, M. R. (2018) Coronavirus Susceptibility to the Antiviral Remdesivir (GS-5734) Is Mediated by the Viral Polymerase and the Proofreading Exoribonuclease. mBio 9, doi.org/10.1128/mBio.00221-18

(2) Shannon, A.; Le, N. T.; Selisko, B.; Eydoux, C.; Alvarez, K.; Guillemot, J. C.; Decroly, E.; Peersen, O.; Ferron, F.; Canard, B. (2020) Remdesivir and SARS-CoV-2: Structural requirements at both nsp12 RdRp and nsp14 Exonuclease active-sites. Antiviral Res. 178, 104793.

(3) De Clercq, E. (2004) Antiviral drugs in current clinical use. J Clin Virol 30, 115-133.

(4) De Clercq, E. (2013) Dancing with chemical formulae of antivirals: A panoramic view (Part 2). Biochem. Pharmacol. 86, 1397-1410.

(5) De Clercq, E. (2013) Dancing with chemical formulae of antivirals: a personal account. Biochem. Pharmacol. 86, 711-725.

(6) Horner, S. M. (2015) Insights into antiviral innate immunity revealed by studying hepatitis C virus. Cytokine 74, 190-197.

(7) Thiel, V.; Ivanov, K. A.; Putics, Á.; Hertzig, T.; Schelle, B.; Bayer, S.; Weißbrich, B.; Snijder, E. J.; Rabenau, H.; Doerr, H. W.; Gorbalenya, A. E.; Ziebuhr, J. (2003) Mechanisms and enzymes involved in SARS coronavirus genome expression. J. Gen. Virol. 84, 2305-2315.

(8) Subissi, L.; Imbert, I.; Ferron, F.; Collet, A.; Coutard, B.; Decroly, E.; Canard, B. (2014) SARS-CoV ORF1b-encoded nonstructural proteins 12-16: replicative enzymes as antiviral targets. Antiviral Res. 101, 122-130.

(9) Minskaia, E.; Hertzig, T.; Gorbalenya, A. E.; Campanacci, V.; Cambillau, C.; Canard, B.; Ziebuhr, J. (2006) Discovery of an RNA virus 3'->5' exoribonuclease that is critically involved in coronavirus RNA synthesis. Proc. Natl. Acad. Sci. U S A 103, 5108-5113.

(10) Freitas, B. T.; Durie, I. A.; Murray, J.; Longo, J. E.; Miller, H. C.; Crich, D.; Hogan, R. J.; Tripp, R. A.; Pegan, S. D. (2020) Characterization and Noncovalent Inhibition of the

Deubiquitinase and deISGylase Activity of SARS-CoV-2 Papain-Like Protease. ACS Infect Dis. doi.org/10.1021/acsinfecdis.0c00168

(11) Frick, D. N.; Virdi, R. S.; Vuksanovic, N.; Dahal, N.; Silvaggi, N. R. (2020) Molecular Basis for ADP-ribose Binding to the Mac1 Domain of SARS-CoV-2 Nsp3 Biochemistry. doi.org/10.1021/acs.biochem.0c00309

(12) Egloff, M. P.; Ferron, F.; Campanacci, V.; Longhi, S.; Rancurel, C.; Dutartre, H.; Snijder, E. J.; Gorbalenya, A. E.; Cambillau, C.; Canard, B. (2004) The severe acute respiratory syndrome-coronavirus replicative protein nsp9 is a single-stranded RNA-binding subunit unique in the RNA virus world. Proc. Natl. Acad. Sci. U S A 101, 3792-3796.

(13) Saikatendu, K. S.; Joseph, J. S.; Subramanian, V.; Clayton, T.; Griffith, M.; Moy, K.; Velasquez, J.; Neuman, B. W.; Buchmeier, M. J.; Stevens, R. C.; Kuhn, P. (2005) Structural basis of severe acute respiratory syndrome coronavirus ADP-ribose-1''-phosphate dephosphorylation by a conserved domain of nsP3. Structure 13, 1665-1675.

(14) Alhammad, Y. M. O.; Fehr, A. R. (2020) The Viral Macrodomain Counters Host Antiviral ADP-Ribosylation. Viruses 12, doi.org/10.3390/v12040384 .

(15) Claverie, J. M. (2020) A Putative Role of de-Mono-ADP-Ribosylation of STAT1 by the SARS-CoV-2 Nsp3 Protein in the Cytokine Storm Syndrome of COVID-19. Viruses 12, doi.org/10.3390/v12060646.

(16) Ericsson, U. B.; Hallberg, B. M.; Detitta, G. T.; Dekker, N.; Nordlund, P. (2006) Thermofluor-based high-throughput stability optimization of proteins for structural studies. Anal. Biochem. 357, 289-298.

(17) Pantoliano, M. W.; Petrella, E. C.; Kwasnoski, J. D.; Lobanov, V. S.; Myslik, J.; Graf, E.; Carver, T.; Asel, E.; Springer, B. A.; Lane, P.; Salemme, F. R. (2001) High-density miniaturized thermal shift assays as a general strategy for drug discovery. J Biomol. Screen. 6, 429-440.

(18) Huynh, K.; Partch, C. L. (2015) Analysis of protein stability and ligand interactions by thermal shift assay. Curr. Protoc. Protein Sci. 79, 28.9.1-28.9.14.

(19) Trott, O.; Olson, A. J. (2010) AutoDock Vina: improving the speed and accuracy of docking with a new scoring function, efficient optimization, and multithreading. J. Comput. Chem. 31, 455-461.

(20) Lee, P. H.; Huang, X. X.; Teh, B. T.; Ng, L. M. (2019) TSA-CRAFT: A Free Software for Automatic and Robust Thermal Shift Assay Data Analysis. SLAS Discov. 24, 606-612.

(21) Cho, C. C.; Lin, M. H.; Chuang, C. Y.; Hsu, C. H. (2016) Macro Domain from Middle East Respiratory Syndrome Coronavirus (MERS-CoV) Is an Efficient ADP-ribose Binding Module: CRYSTAL STRUCTURE AND BIOCHEMICAL STUDIES. J. Biol. Chem. 291, 4894-4902.

(22) Malet, H.; Coutard, B.; Jamal, S.; Dutartre, H.; Papageorgiou, N.; Neuvonen, M.; Ahola, T.; Forrester, N.; Gould, E. A.; Lafitte, D.; Ferron, F.; Lescar, J.; Gorbalenya, A. E.; de Lamballerie, X.; Canard, B. (2009) The crystal structures of Chikungunya and Venezuelan equine encephalitis virus nsP3 macro domains define a conserved adenosine binding pocket. J. Virol. 83, 6534-6545.

(23) Larsson, E. A.; Jansson, A.; Ng, F. M.; Then, S. W.; Panicker, R.; Liu, B.; Sangthongpitag, K.; Pendharkar, V.; Tai, S. J.; Hill, J.; Dan, C.; Ho, S. Y.; Cheong, W. W.; Poulsen, A.; Blanchard, S.; Lin, G. R.; Alam, J.; Keller, T. H.; Nordlund, P. (2013) Fragment-based ligand design of novel potent inhibitors of tankyrases. J. Med. Chem. 56, 4497-4508.

(24) Li, K.; Frankowski, K. J.; Belon, C. A.; Neuenswander, B.; Ndjomou, J.; Hanson, A. M.; Shanahan, M. A.; Schoenen, F. J.; Blagg, B. S.; Aubé, J.; Frick, D. N. (2012) Optimization of potent hepatitis C virus NS3 helicase inhibitors isolated from the yellow dyes thioflavine S and primuline. J. Med. Chem. 55, 3319-3330.

(25) Mukherjee, S.; Weiner, W. S.; Schroeder, C. E.; Simpson, D. S.; Hanson, A. M.; Sweeney, N. L.; Marvin, R. K.; Ndjomou, J.; Kolli, R.; Isailovic, D.; Schoenen, F. J.; Frick, D. N. (2014) Ebselen inhibits hepatitis C virus NS3 helicase binding to nucleic acid and prevents viral replication. ACS Chem. Biol. 9, 2393-2403.

(26) Zhang; Chung; Oldenburg (1999) A Simple Statistical Parameter for Use in Evaluation and Validation of High Throughput Screening Assays. J. Biomol. Screen. 4, 67-73.

(27) Rothlin, R. P.; Vetulli, H. M.; Duarte, M.; Pelorosso, F. G. (2020) Telmisartan as tentative angiotensin receptor blocker therapeutic for COVID-19. Drug Dev. Res. doi.org/10.1002/ddr.21679

(28) Grandi, G.; Facchinetti, F.; Bitzer, J. (2020) The gendered impact of coronavirus disease (COVID-19): do estrogens play a role Eur J Contracept Reprod Health Care 25, 233-234.

(29) Breithaupt-Faloppa, A. C.; Correia, C. J.; Prado, C. M.; Stilhano, R. S.; Ureshino, R. P.; Moreira, L. F. P. (2020) 17β-Estradiol, a potential ally to alleviate SARS-CoV-2 infection. Clinics (Sao Paulo) 75, e1980.

(30) Paluri, R. K.; Kasi, A.; Young, C.; Posey, J. A. (2020) Second-line treatment for metastatic pancreatic cancer. Clin. Adv. Hematol. Oncol. 18, 106-115.

(31) Zhou, Y.; Hou, Y.; Shen, J.; Huang, Y.; Martin, W.; Cheng, F. (2020) Network-based drug repurposing for novel coronavirus 2019-nCoV/SARS-CoV-2. Cell Discov. 6, 14.

(32) Layton, C. J.; Hellinga, H. W. (2010) Thermodynamic analysis of ligand-induced changes in protein thermal unfolding applied to high-throughput determination of ligand affinities with extrinsic fluorescent dyes. Biochemistry 49, 10831-10841.

(33) Wazir, S.; Maksimainen, M. M.; Alanen, H. I.; Galera-Prat, A.; Lehtiö, L. (2020) Activity-Based Screening Assay for Mono-ADP-Ribosylhydrolases. SLAS Discov. doi.org/10.1177/2472555220928911.

(34) Jankevicius, G.; Hassler, M.; Golia, B.; Rybin, V.; Zacharias, M.; Timinszky, G.; Ladurner, A. G. (2013) A family of macrodomain proteins reverses cellular mono-ADP-ribosylation. Nat. Struct. Mol. Biol. 20, 508-514.

(35) Li, C.; Debing, Y.; Jankevicius, G.; Neyts, J.; Ahel, I.; Coutard, B.; Canard, B. (2016) Viral Macro Domains Reverse Protein ADP-Ribosylation. J. Virol. 90, 8478-8486.

(36) Haikarainen, T.; Maksimainen, M. M.; Obaji, E.; Lehtiö, L. (2018) Development of an Inhibitor Screening Assay for Mono-ADP-Ribosyl Hydrolyzing Macrodomains Using AlphaScreen Technology. SLAS Discov. 23, 255-263.

(37) Alhammad, Y. M. O.; Kashipathy, M. M.; Roy, A.; Johnson, D. K.; McDonald, P.; Battaile, K. P.; Gao, P.; Lovell, S.; Fehr, A. R. (2020) The SARS-CoV-2 conserved macrodomain is a highly efficient ADP-ribosylhydrolase enzyme. bioRxiv. doi.org/10.1101/2020.05.11.089375

(38) Daniels, C. M.; Thirawatananond, P.; Ong, S. E.; Gabelli, S. B.; Leung, A. K. (2015) Nudix hydrolases degrade protein-conjugated ADP-ribose. Sci Rep 5, 18271.

(39) Dunn, C. A.; O'Handley, S. F.; Frick, D. N.; Bessman, M. J. (1999) Studies on the ADP-ribose pyrophosphatase subfamily of the nudix hydrolases and tentative identification of trgB, a gene associated with tellurite resistance. J. Biol. Chem. 274, 32318-32324.

(40) Patel, P.; Sengupta, N. (2020) PPIs and Beyond: A Framework for Managing Anticoagulation-Related Gastrointestinal Bleeding in the Era of COVID-19. Dig Dis Sci. doi.org/10.1007/s10620-020-06408-x.

(41) Shimizu, J. F.; Martins, D. O. S.; McPhillie, M. J.; Roberts, G. C.; Zothner, C.; Merits, A.; Harris, M.; Jardim, A. C. G. (2020) Is the ADP ribose site of the Chikungunya virus NSP3 Macro domain a target for antiviral approaches Acta Trop. 207, 105490.

(42) Pettersen, E. F.; Goddard, T. D.; Huang, C. C.; Couch, G. S.; Greenblatt, D. M.; Meng, E. C.; Ferrin, T. E. (2004) UCSF Chimera--a visualization system for exploratory research and analysis. J. Comput. Chem. 25, 1605-1612.

Table I. **Effects of various nucleotides on SARS-CoV-2 Mac1.** $\Delta T_{m\ max}$ and EC_{50} values obtained in concentration response assays using the DSF assay compared with previously published results obtained with ITC.[11]

Compounds	$\Delta T_{m\ max}$ ***(°C)***	EC_{50} ***(µM)***	K_d ***(ITC)***
ADP-ribose	7±0.9	63 ± 21	10±6
ADP-glucose	~2 @ 500 µM	> 500	9.5±5
ADP	6.2±1	314 ±43	3.4±0.6
ATP	5.6 ±0.7	483 ± 129	2.4±1
AMP	~2 @ 500 µM	> 500	N.D.
cAMP	1.9 ± 0.8	746 ± 340	6.1±
NADH	5.8 ±0.4	410 ± 76	44±20

Class	***NAME***	*ΔT_m (°C)*	*VINA Energy*	*EC_{50} (μM)*	*K_d (μM)*	*N*[a]	*ΔH (kJ/mol)*	*ΔS (J/mol·K)*
Steriods	Estradiol Valerate	31	-9.8	100	N.D.			
	Flunisolide	17	-8.5	>500	N.D.			
Lactams	Cefaclor	-3	-8.1	376	N.D.			
	Cefatrizine	-5	-9	4	N.D.			
Benzimidazoles	Telmisartan	28	-11.4	>500	N.D.			
	Rabeprazole	-4	-7.7	195	68±28	0.7±0.5	-91±44	-228
	Omeprazole	-3	-6.8	40	96±181	2.3±2.1	-16±77	21
	Esomeprazole	-3	-8.1	>500	N.D.			
Others	Irinotecan	1	-10.1	>500	20±20	3.4±0.4	-5.8±1.3	70
	Nifedipine	-6	-7.1	>500	50±41	1.6±0.8	-14±30	35
	Trifluoperazine	-3	-8.3	>500	30±18	1.8±0.3	-25±7	1.5
Control	ADP-ribose	7		63	15±4	0.9±0.3	-91±21	-215

Table II. **Summary of results obtained with select hits from the DSF and virtual screens**

[a]Stoichiometry (ligands/protein). N.D. Binding not detected with ITC.

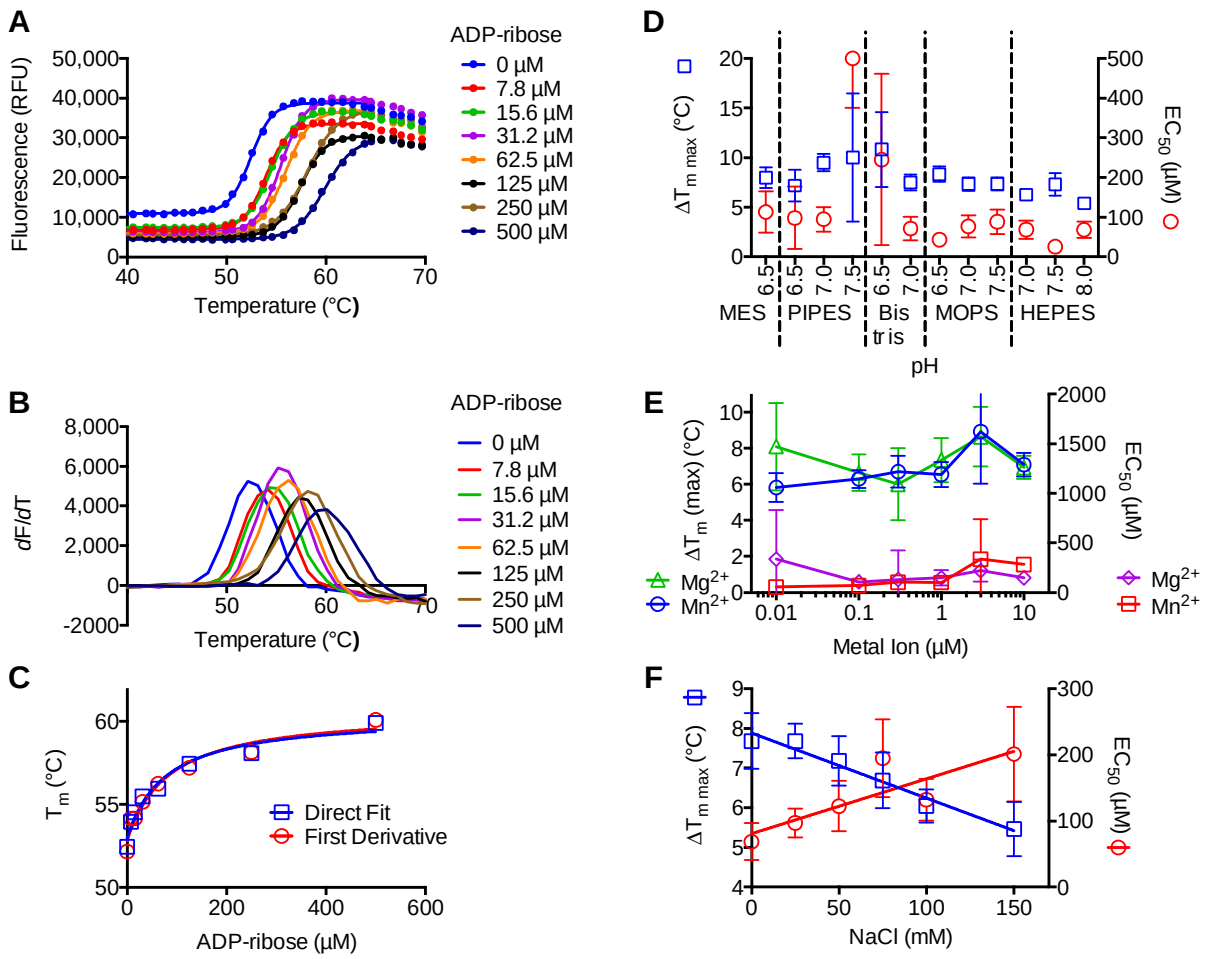

Figure 1. **DSF assay optimization.** (A) SPYRO Orange fluorescence in the presence of 6 µM Mac1 protein at various temperatures in the presence of indicated concentrations of ADP-ribose. Data are fit to Eq. 1 using non-linear regression with GraphPad Prism. (B) The first derivative of the data in panel A plotted vs temperature. (C) T_m values obtained from either the peaks of the first derivative plots (circles) or from direct fitting to Eq. 1 (squares). Data are fit to Eq. 2. (D) The same titrations with ADP-ribose shown in Panels A-C were repeated in various buffers at a range of pH values (x-axis). Plotted are best-fit $\Delta T_{m\ max}$ (squares, left y-axis) and EC_{50} (circles, right axis) values obtained when observed T_m values were fit to Eq. 2 (methods). Error bars mark standard errors in the curve fits. (E) Titrations with ADP-ribose performed in 20 mM MOPS buffer pH 7 in the presence of indicated divalent metal cation concentrations, supplied as $MgCl_2$ (triangles, diamond) or $MnCl_2$ (circles, squares). Plotted are best-fit $\Delta T_{m\ max}$ (triangles, circles, left y-axis) and EC_{50} (diamonds, squares, right axis) values obtained when observed T_m values were fit to Eq. 2 (methods). Error bars mark standard errors in the curve fits. (F) ADP-ribose titrations in 20 mM MOPS pH buffer supplemented with indicated NaCl concentrations. Plotted are best-fit $\Delta T_{m\ max}$ (squares, left y-axis) and EC_{50} (circles, right axis) values obtained when observed T_m values were fit to Eq. 2. Error bars mark standard errors in the curve fits.

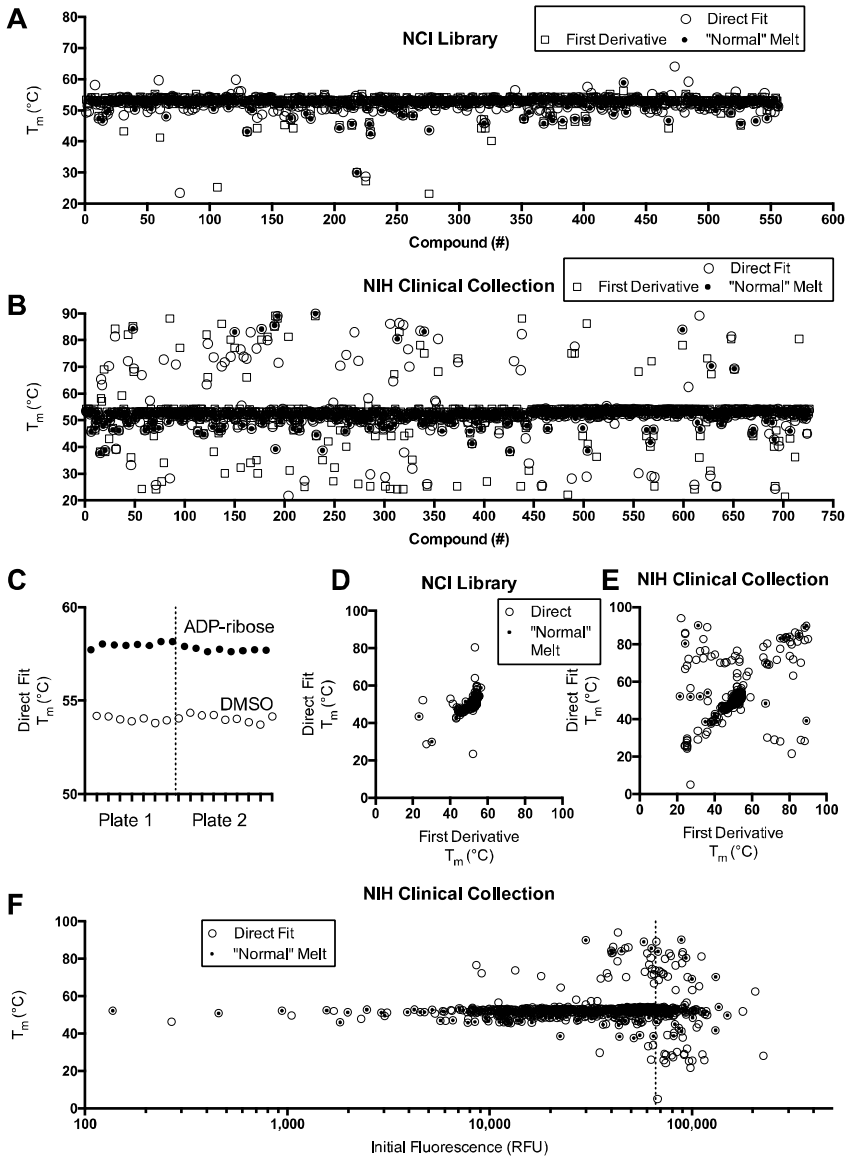

Figure 2. **DSF screens of FDA-approved drugs and drug-like compounds for SARS-CoV-2 Mac1 ligands.** (A) T_m values obtained for each compound in the NCI library calculated using either the first derivative method (squares) or direct fits to Eq. 1 (circles). Assays yielding a normal melting curve, as defined by the TSA-CRAFT algorithm are noted with filled circles. (B) Results from assays performed with compounds in the NIH clinical collection plotted as described in panel A. (C) T_m values for positive and negative controls from two different 96-well plates (Z' factor = 0.72). (D, E) Correlation plots comparing T_m values calculated using either the direct fit method (TSA-CRAFT, Eq. 1) or first derivative method for either the NCI library (D) or NIH clinical collection (E). Samples which TSA-CRAFT identified as normal melting curves are highlighted as filled circles in D and E. (F) Plot of T_m values obtained using TSA-CRAFT for samples in the NIH clinical collection plotted versus fluorescence observed at the beginning of each melt (*i.e.* @ 20 °C). Note the x-axis is a log scale, and normal melting curves are highlighted as filled circles. The dotted line is an arbitrary cutoff drawn at three times the average fluorescence intensity recorded in all assays.

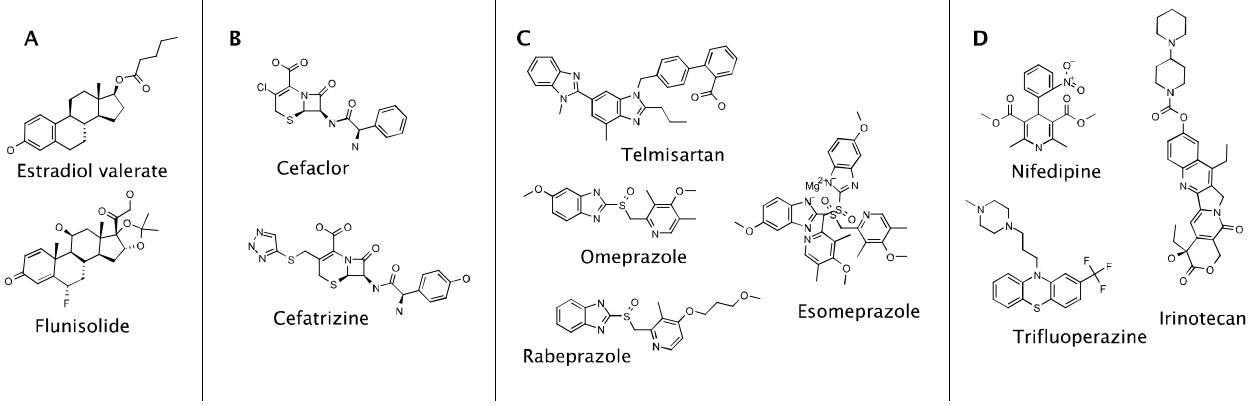

Figure 3. **Selected hit compounds from the NIH clinical collection.** (A) Steroids at raise the apparent T_m of SARS-CoV-2 Mac1. (B) Two lactam antibiotics that lowered the apparent T_m of SARS-CoV-2 Mac1. (C) Benzimidazoles altering the SARS-CoV-2 Mac1 T_m (D) three additional hits for which binding could be confirmed using ITC.

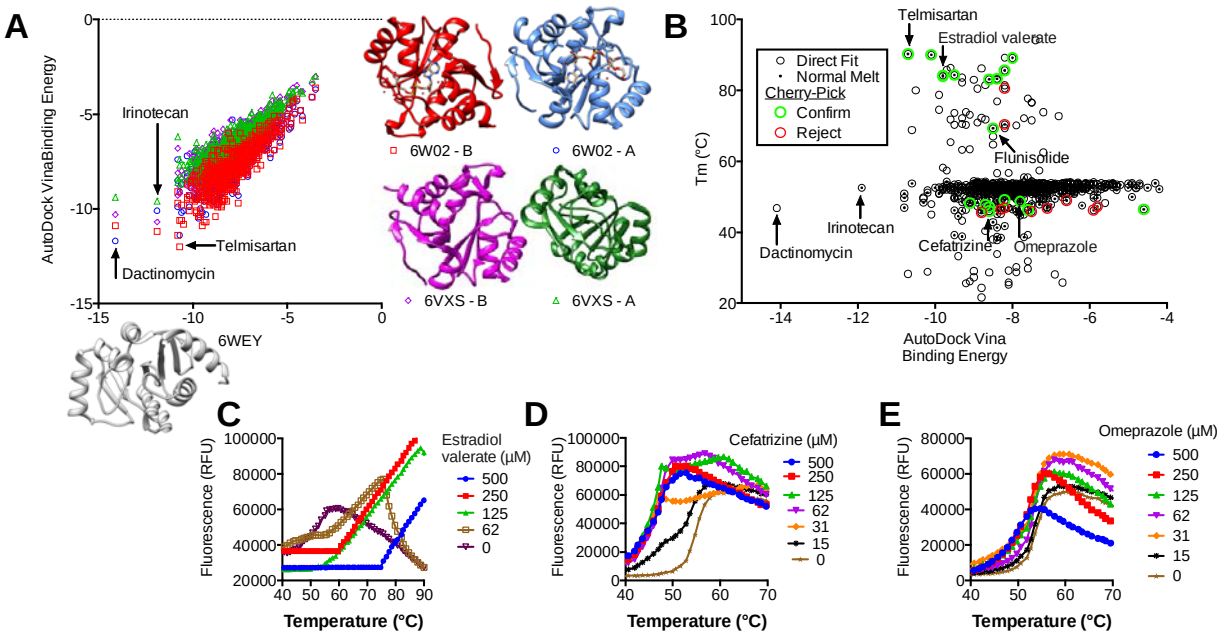

Figure 4. **Virtual screening of the NIH clinical collection.** (A) AutoDock Vina binding energies obtained for each compound after docking with PDB file 6WEY (x-axis) compare to binding energies when each compound was docked with BioAssembly A of 6W02 (circles) BioAssembly B of 6W02 (squares), BioAssembly A of 6VXS (triangles) and BioAssembly B of 6VXS (diamonds). (B) AutoDock Vina binding energies obtained for each compound after docking with PDB file 6WEY (y-axis) compared with the T_m derived using TSA-CRAFT (see Fig. 2). Compounds selected for follow-up (cherry pick) analysis are highlighted. (C-E) Concentration response analysis of three selected compounds (see text for details).

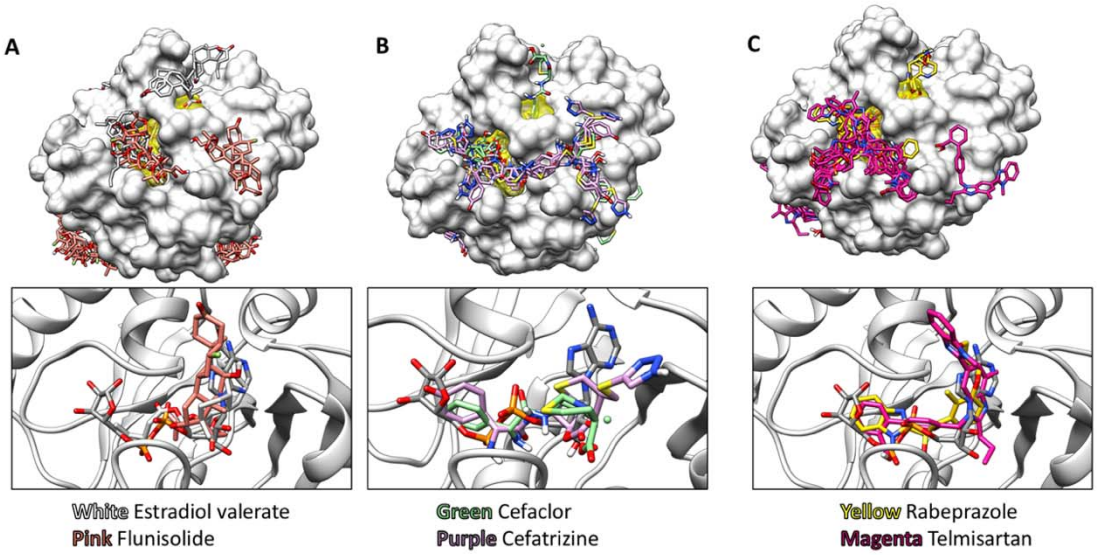

Figure 5. **Representative Structures obtained using AutoDock Vina Virtual Screening.** Top panels show the top 20 binding modes for selected compounds, and the bottom panels show the top binding mode for each compound compared to the ADP-ribose bound in PDB file 6W02. The ADP-ribose binding cleft is highlighted in yellow on the protein surfaces shown in the top panels. Results are shown for (A) two steroids, (B) two lactam antibiotics, and (C) two benzimidazoles in the NIH clinical collection. Structures are displayed using *UCSF-Chimera*.[42]

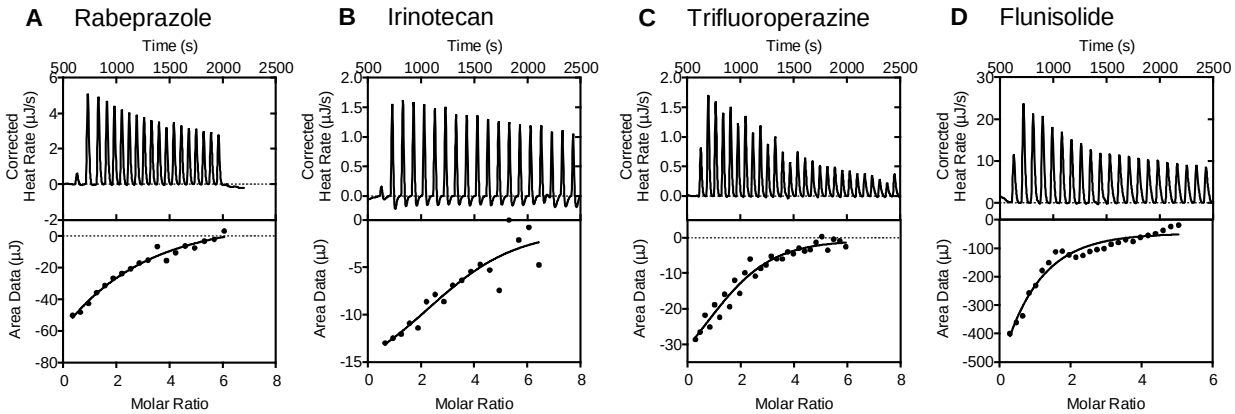

Fig. 6. **ITC results with selected compounds from the NIH clinical collection.** Example ITC experiment in which the purified SARS-CoV-2 Mac1 titrated with (A) Rabeprazole (B) nifedipine (C) trifluoroperazine, and (D) irinotecan. Best fit parameters are summarized in Table II.